

# $\sin^2 \theta_W$ estimate and neutrino electromagnetic properties from low-energy solar data

Amir N. Khan\*

*Max-Planck-Institut für Kernphysik, Saupfercheckweg 1, 69117 Heidelberg, Germany and  
Theoretical Physics Department, Fermi National Accelerator Laboratory, P.O. Box 500, Batavia, IL 60510, USA*

(Dated: February 19, 2019)

We report new values of weak-mixing angle ( $\sin^2 \theta_W$ ), neutrino effective magnetic moment ( $\mu_V^{eff}$ ) and the charge radii ( $\langle r_{V\alpha}^2 \rangle$ ) using the lowest-energy (to-date) solar neutrino data of pp,  ${}^7\text{Be}$  and pep spectra from phase-I and phase-II runs of Borexino experiment. The best-fit values obtained are  $\sin^2 \theta_W = 0.235 \pm 0.019$  at  $1\sigma$  with a precision comparable to that of the combined reactor and accelerator very short-baseline experiments and  $\mu_V^{eff} \leq 8.7 \times 10^{-12} \mu_B$  at 90% C.L. with a factor of 3 improvement over the previous bounds. This leads to the improvement of constraints on all the related magnetic moment matrix elements for the Majorana-type and Dirac-type neutrinos in mass basis and also stronger bounds on the magnetic moment flavor states. The bounds on the neutrino charge radii obtained are  $0.82 \times 10^{-32} \text{cm}^2 \leq \langle r_{V_e}^2 \rangle \leq 1.27 \times 10^{-32} \text{cm}^2$  and  $-9 \times 10^{-32} \text{cm}^2 \leq \langle r_{V\mu, V\tau}^2 \rangle \leq 3.1 \times 10^{-31} \text{cm}^2$  at 90% C.L..

## I. INTRODUCTION

Tests of the Standard Model (SM) of particle physics, and the corresponding determination of its characteristic electroweak parameters, span many orders of magnitude in energy. The measurements of the scale dependence of the fundamental electroweak parameter  $\sin^2 \theta_W$  now cover the range from 10 TeV at the Large Hadron Collider CMS [1], ATLAS [2], LHCb [3] to a few MeV and below at Solar neutrino detectors SNO [4], KamLAND [5], Borexino [6–9] and atomic spectral measurements of electroweak parity violation in  ${}^{133}\text{Cs}$  [10–12]. In between, in the range from multi-MeV to multi-GeV is a host of experiments in operation or development designed to look for deviations from the SM in the form of lepton flavor and universality violations [13–15] and to make precision measurements in the process (Belle, BelleII, BaBar)[16], Q-weak [17, 18], SoLID [19], MOLLER [20]. At present the lowest energy determination of  $\sin^2 \theta_W$  is that provided by the parity-violation measurement in  ${}^{133}\text{Cs}$  at 2.4 MeV [10–12] and in the lowest possible energy solar data at 1.4MeV and below has been estimated in ref. [21].

In the low energy regime ( $\leq 100\text{MeV}$ ), the neutrino interactions in scattering off electrons have played a key role in understanding the gauge structure, precision test of the standard model and in looking for new physics like the electromagnetic properties and nonstandard interactions of neutrino [21, 22]. On the other hand, the neutrino oscillation experiments have also entered into the precision era of the oscillation parameters [23–25]. As the oscillation parameters get more and more precise, the experimental outputs give as a by-product several other interesting precision tests of the SM parameters including  $\sin^2 \theta_W$  and increase the room new physics such as electromagnetic properties and the nonstandard interactions of neutrinos as recently been explored in ref. [21] for Phase-II data of Borexino’s measurements.

The low-energy neutrinos scattering off the electrons elastically are ideal sources for measuring the value of  $\sin^2 \theta_W$  and for exploring the electromagnetic properties of neutrinos [26]. Here we focus on low energy neutrino-electron scattering as a probe for new features in electroweak physics beyond the standard model. SM loop calculations predict that the neutrinos have finite, but exceedingly small, magnetic moment and charge radius. At tree level, their only interaction with the electron is purely weak and short range, while the higher order electromagnetic cross section is long range, inversely proportional to the electron recoil energy. This kinematic feature enhances the photon exchange in low energy neutrino-electron scattering compared to exchange of the weak bosons and makes neutrino-electron scattering an ideal, sensitive testing ground for this new physics, which shows up as anomalous distortions of the electron recoil spectrum. It is this feature that we pursue with the pp (0-0.480MeV),  ${}^7\text{Be}$ (0.86MeV) and pep (1.4MeV) data at the very low end of the solar neutrino spectrum, detected by Borexino’s clean electron recoil detection system in phase I [6–8] and phase II [9] runs and use it for the precision test of  $\sin^2 \theta_W$  and for the study of electromagnetic properties.

---

\*Electronic address: ntrnphysics@gmail.com; Electronic address: akhan@fnal.gov

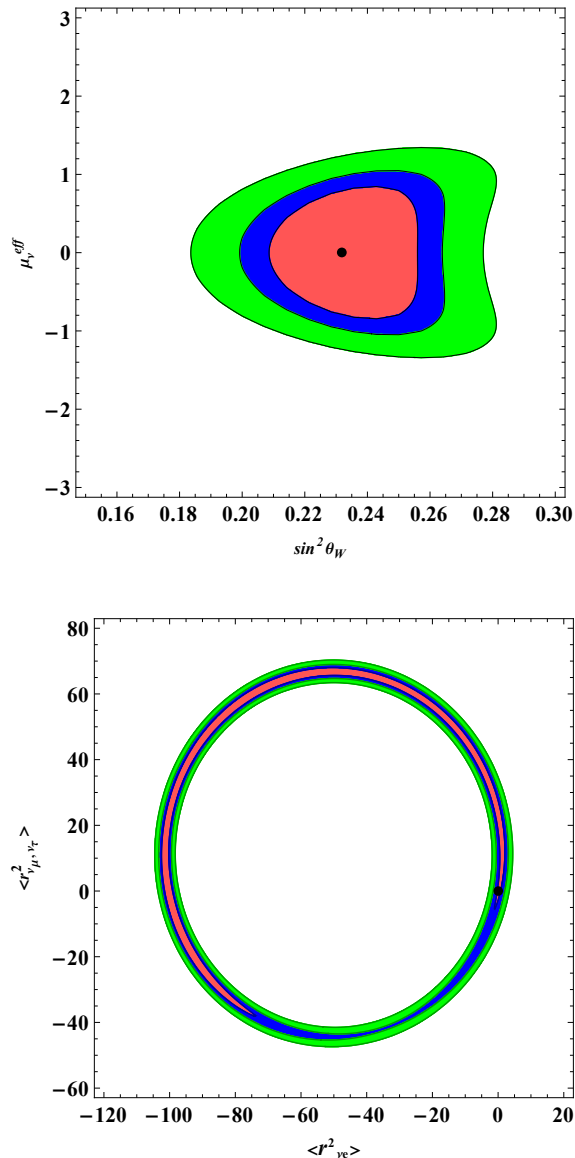


FIG. 1: The 2-*d.o.f* parameter space of weak-mixing angle and effective magnetic moment (upper) and charge radius of  $\nu_e$  versus the charge radius of  $\nu_\mu$  or  $\nu_\tau$  (lower) using the solar low-energy data of  $pp$ ,  ${}^7\text{Be}$ ,  $pep$  reactions at Borexino phase-I and phase-II runs. The red, blue, green regions are 1 $\sigma$  and 90%, 95% C.L. boundaries. The black dot shows the best-fit points. The scale of  $\mu_\nu^{eff}$  is in units of  $\times 10^{-11} \mu_B$  and for the charge radii is in  $\times 10^{-32} \text{cm}^2$ .

In the next section, we review the formalism for  $\nu_\alpha e$ – electroweak scattering process in the presence of electromagnetic diagram and in sections III and IV we discuss the solar neutrino oscillation probabilities on Earth and the neutrino magnetic moments in the flavor and mass basis both for Dirac and Majorana type neutrinos, respectively. Section V is dedicated to the analysis details and to the obtained results while we conclude this study in section VI.

## II. $\nu_\alpha e^-$ SCATTERING CROSS-SECTIONS

The differential cross-sections for the three processes of  $\nu_e e^-$ ,  $\nu_\mu e^-$  and  $\nu_\tau e^-$  scatterings are the incoherent sums of the standard model weak and the electromagnetic interaction differential cross-sections. After integration over the recoiled electron energy ( $T$ ), the total cross-sections read [26]

$$\sigma_{tot} = \int_0^{T_{max}} \left[ \left( \frac{d\sigma_{\nu e}}{dT} \right)_{SM} + \left( \frac{d\sigma_{\nu e}}{dT} \right)_{em} \right] dT, \quad (1)$$

where

$$\left( \frac{d\sigma_{\nu e}}{dT} \right)_{SM} = \frac{2G_F^2 m_e}{\pi} [g_L^2 + g_R^2 \left( 1 - \frac{T}{E_\nu} \right)^2 - g_L g_R \frac{m_e T}{E_\nu^2}] \quad (2)$$

and

$$\left( \frac{d\sigma_{\nu e}}{dT} \right)_{em} = \frac{\pi \alpha_{em}^2 (\mu_\nu^{eff})^2}{m_e^2 \mu_B^2} \left[ \frac{1}{T} - \frac{1}{E_\nu} \right]. \quad (3)$$

Here

$$g_L = (g_V + g_A)/2 + 1, \quad g_R = (g_V - g_A)/2$$

for  $\nu_e$  and

$$g_L = (g_V + g_A)/2, \quad g_R = (g_V - g_A)/2$$

for  $\nu_\mu$  and  $\nu_\tau$ , where  $g_V = -1/2 + 2 \sin^2 \theta_W$  and  $g_A = -1/2$ ,  $\mu_\nu^{eff}$  is the effective neutrino magnetic moment,  $\mu_B$  is the Bohr magneton unit,  $\alpha_{em}$  is the fine-structure constant,  $m_e$  is the electron mass,  $E_\nu$  is the neutrino energy and  $T_{max}$  is the maximum recoiled-electron energy in the detector.  $T_{max}(E_\nu) \equiv E_\nu / (1 + m_e/2E_\nu)$ , where  $0 < E_\nu < 0.420$  MeV for  $pp$  events and  $E_\nu = 0.862$  MeV and  $1.44$  MeV for  ${}^7\text{Be}$  and  $pep$  events, respectively. Notice that the term "1" in the definition of  $g_L$  for  $\nu_e$  corresponds to the CC contribution in the  $\nu_e - e$  scattering.

Neutrinos are electrically neutral particles in the standard model, their electric form factors in terms of neutrino charge radius can still give useful information about the electromagnetic properties. In the earlier studies, it was claimed that neutrino charge radius is not a physical quantity because of the ultraviolet-divergences produced in the unitary gauge [28] or in general gauge [29, 30] in one-loop and  $\gamma - Z$  self-energy calculations. These infinities can be cured using the unitary gauge if the neutrino-lepton neutral current contribution is added to usual terms, then for the neutrino charge radius a finite gauge-dependent quantity can be obtained [31]. In order to calculate the neutrino charge radius as a finite gauge-independent physical quantity, one has to add box diagram contribution to the tree level diagrams of the neutrino-lepton scattering processes [32]. The neutrino charge radius can thus be introduced as gauge-independent physical observable in the calculations of one-loop approximation including the additional terms from the  $\gamma - Z$  boson mixing and the box diagrams of W and Z bosons [33–35] as

$$\langle r_{\nu_\alpha}^2 \rangle = \frac{G_F}{4\sqrt{2}\pi^2} [3 - 2 \log(\frac{m_\alpha^2}{m_W^2})] \quad (4)$$

where  $m_W$  is the W-boson mass and  $m_\alpha$  ( $\alpha = e, \mu, \tau$ ) denotes the masses of charged leptons and  $G_F$  is the Fermi constant.

In order to see the effects of the neutrino charge radius, one can modify the definition of  $g_V$  as  $g_V = \sin^2 \theta_w - 1/2 + (2\sqrt{2}\alpha_{em}/3G_F) \langle r_{\nu_e}^2 \rangle$  for  $\nu_e - e$  scattering and  $g_V = \sin^2 \theta_w - 1/2 + (2\sqrt{2}\alpha_{em}/3G_F) \langle r_{\nu_\mu, \nu_\tau}^2 \rangle$  for  $\nu_\mu e^-$  or  $\nu_\tau e^-$  scatterings [26] as was done in ref. [36] for the reactor data.

Parameter	$\sin^2 \theta_W$	$\mu_\nu^{eff}$	$\langle r_{\nu_e}^2 \rangle$	$\langle r_{\nu_\mu, \nu_\tau}^2 \rangle$
This work	$0.235 \pm 0.019$	$\leq 8.7 \times 10^{-12} \mu_B$	$[-0.82, 1.27] \times 10^{-32} \text{cm}^2$	$[-9, 31] \times 10^{-32} \text{cm}^2$
Prediction	$0.23867 \pm 0.00016$ [37]	$\leq 10^{-18} \mu_B$ [27]	$4.1 \times 10^{-33} \text{cm}^2$ [27]	$(2.4, 1.5) \times 10^{-33} \text{cm}^2$ [27]

TABLE I: Best-fit value of weak mixing angle with  $1\sigma$  uncertainty, upper bound on neutrino effective magnetic moment and bounds on charge radii of  $\nu_e$  and  $\nu_\mu$  or  $\nu_\tau$  at 90% C.L. obtained from the one parameter at-a-time  $\Delta\chi^2$  distributions of Fig. 2. The 3<sup>rd</sup> row shows predicted values. The neutrino effective magnetic moment value is calculated in the minimally-extended standard model with massive Dirac neutrinos using the current bound on the neutrino mass. The predicted value for  $\sin^2 \theta_W$  is the  $\overline{MS}$  running parameter value taken from PDG2016 [37].

### III. SOLAR NEUTRINO OSCILLATION PROBABILITIES AT EARTH

For low-energy solar neutrino spectra of  $pp$ ,  ${}^7\text{Be}$  and  $pep$ , the LMA-MSW expectation is that the mixing at Earth is essentially due to the vacuum oscillations. In this case the oscillation amplitude takes the matrix form  $A_{\alpha\beta} = U_{\alpha a} X_a U_{a\beta}^\dagger$ , where  $a, b, c, \dots$  are the mass basis indices and  $\alpha$  and  $\beta$  are the flavor basis indices (summation over repeated indices is implied). The  $U$  matrix is the neutrino mass mixing matrix for any number of neutrinos and  $X$  is the diagonal phase matrix  $X = \text{diag}(1, \exp(-i2\pi L/L_{21}^{osc}), \exp(-i2\pi L/L_{31}^{osc}), \dots)$ , where the oscillation length is defined as  $L_{ab}^{osc} = 4\pi E / (m_a^2 - m_b^2)$ . The oscillation probability reads as

$$P_{\alpha\beta} = |A_{\alpha\beta}|^2 = |U_{\alpha a} X_a U_{a\beta}^*|^2, \quad (5)$$

so the average over an oscillation length is then

$$\langle P \rangle_{\alpha\beta} = U_{\alpha a} U_{\beta a}^* U_{a\alpha}^* U_{a\beta} = |U_{\alpha a}|^2 |U_{\beta a}|^2, \quad (6)$$

for the average over one cycle of the probability function. For instance, for the  $3 \times 3$  mixing in vacuum, the electron survival averaged probability is  $\langle P \rangle_{ee} = s_{13}^4 + (c_{12}c_{13})^4 + (s_{12}c_{13})^4$ , where  $s_{ij} \equiv \sin \theta_{ij}$  and  $c_{ij} \equiv \cos \theta_{ij}$ .

For these lowest energy solar neutrinos of  $pp$  reaction with energy  $E_\nu \leq 0.420$  MeV, the matter effects on the probability ( $P_{ee}$ ) that a  $\nu_e$  survives as  $\nu_e$  in the trip from the core of the Sun to the detector are negligible, less than a percent different from the path-averaged over the oscillation length, thus they are pure vacuum-mixing predictions. However, for the somewhat higher energy line spectra of  ${}^7\text{Be}$  (0.862 MeV) and  $pep$  (1.44 MeV) neutrinos, the matter effects are still small, upto 4-5%, but not entirely negligible. Therefore, we include the small modifications due to matter effects to the purely vacuum value of  $\langle P_{ee} \rangle$ . For this purpose in the  $3 \times 3$  scenario, the LMA-Wolfenstein matter effects modify the vacuum oscillation probabilities of  ${}^7\text{Be}$  and  $pep$  neutrinos as

$$\langle P^m \rangle_{ee} = s_{13}^4 + \frac{1}{2} c_{13}^4 (1 + \cos 2\theta_{12}^m \cos 2\theta_{12}), \quad (7)$$

where

$$\cos 2\theta_{12}^m = \frac{1 - N_e/N_e^{res}}{\sqrt{(1 - N_e/N_e^{res})^2 + \tan^2 2\theta_{12}}} \quad (8)$$

is the effective mixing angle inside the sun,  $N_e$  is the electron number density at the center of the sun,  $N_e^{res} = \Delta m_{12}^2 \cos 2\theta_{12} / 2E_\nu \sqrt{2} G_F$  is the electron density in the resonance region and  $\Delta m_{12}^2$  is the solar mass-squared difference,  $\theta_{12}$  is the solar mixing angle. For  $pp$  spectrum, we use electron density at average  $pp$  neutrino energy and production point in the above expressions [38] and then assuming an exponential decrease in the density outward from the core in the analytic approximations as discussed in detail in ref. [38]. It is an excellent approximation for  $r > 0.1 R_{solar}$  [39].

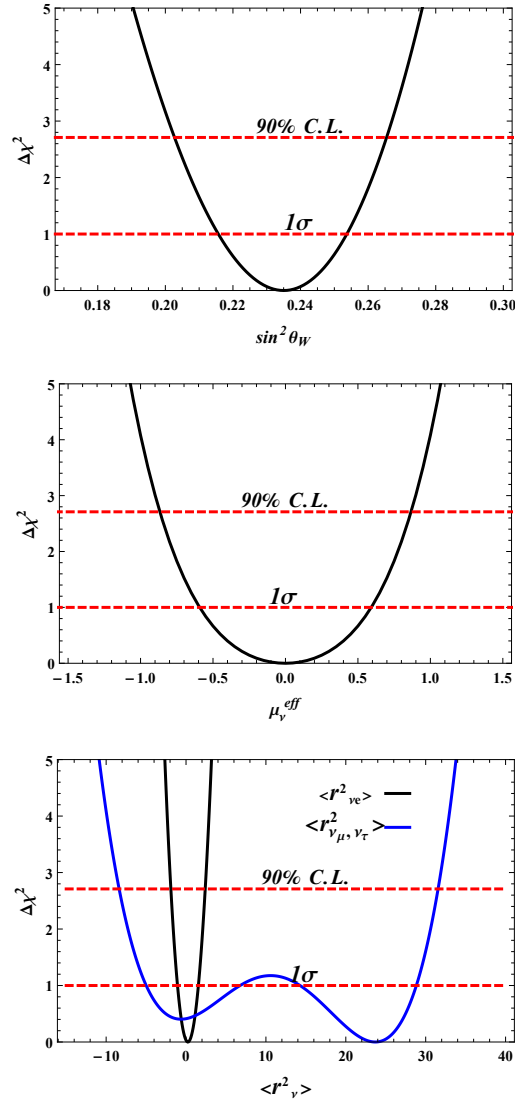


FIG. 2: The 1 parameters  $\Delta\chi^2$ -distributions of weak-mixing angle (top), effective magnetic moment (middle) and the neutrino charge radii of  $\nu_e$ ,  $\nu_\mu$  or  $\nu_\tau$  (bottom) using the solar low-energy data of  $pp$ ,  ${}^7\text{Be}$ ,  $pep$  reactions at Borexino phase I and II runs. From bottom to top, the  $1\sigma$  and 90% C.L. projections are shown by red dashed lines. The scale of  $\mu_\nu^{eff}$  is in units of  $\times 10^{-11}\mu_B$  and that of  $\langle r^2_\nu \rangle$  is in  $\times 10^{-32}\text{cm}^2$ .

#### IV. NEUTRINO MAGNETIC MOMENTS IN MASS AND FLAVOR BASIS

In the mass-basis, for the Dirac-type neutrinos the effective magnetic moment have only non-zero diagonal matrix elements while for Majorana-type of neutrinos, the off-diagonal matrix elements are only relevant [27, 40–42]. Thus, the neutrinos effective magnetic moment can be written in terms of the Dirac- and Majorana-type magnetic moment matrix elements in the mass-basis as

$$(\mu_{eff}^D)^2 = P_{e1}^{3\nu}\mu_{11}^2 + P_{e2}^{3\nu}\mu_{22}^2 + P_{e3}^{3\nu}\mu_{33}^2 \quad (9)$$

$$(\mu_{eff}^M)^2 = (P_{e1}^{3\nu} + P_{e2}^{3\nu})\mu_{12}^2 + (1 - P_{e2}^{3\nu})\mu_{13}^2 + (1 - P_{e1}^{3\nu})\mu_{23}^2. \quad (10)$$

Notice that we have obtained this form of eq. (9) and (10) after applying the unitarity condition,  $\sum_{i=1}^3 P_{ei} = 1$ , and assuming the CPT invariance ( $\mu_{ij} = \mu_{ji}$ ), where  $P_{e1}^{3\nu} = c_{13}^2 P_{e1}^{2\nu}$ ,  $P_{e2}^{3\nu} = c_{13}^2 P_{e2}^{2\nu}$ ,  $P_{e3}^{3\nu} = s_{13}^2$ ,  $P_{e1}^{2\nu}$  and  $P_{e2}^{2\nu}$  are the effective

Flux	$ \mu_{11} $	$ \mu_{22} $	$ \mu_{33} $	$ \mu_{12} $	$ \mu_{13} $	$ \mu_{23} $	$ \mu_e $	$\mu_\mu$	$ \mu_\tau $
pp	1.05	1.58	5.94	8.60	1.04	1.52	1.17	1.73	1.96
${}^7\text{Be}$	1.09	1.47	5.94	8.60	1.07	1.43	1.18	1.70	1.93
pep	1.10	1.44	5.94	8.60	1.08	1.40	1.19	1.69	1.91

TABLE II: In the mass-basis, Dirac-type column (1-3), Majorana-type column (4-6) and in the flavor basis (7-9) magnetic moments in units of  $\times 10^{-11} \mu_B$  derived from effective magnetic moment as shown in Fig. 1, for  $pp$ ,  ${}^7\text{Be}$  and  $pep$  of Borexino phase-I and phase-II runs.

2-neutrino solar oscillation probabilities in the LMA-MSW solution [43]. Eq. (9) and (10) can be rewritten as

$$(\mu_{eff}^D)^2 = c_{13}^2 P_{e1}^{2\nu} \mu_{11}^2 + c_{13}^2 P_{e2}^{2\nu} \mu_{22}^2 + s_{13}^2 \mu_{33}^2 \quad (11)$$

$$(\mu_{eff}^M)^2 = c_{13}^2 \mu_{12}^2 + (1 - c_{13}^2 P_{e2}^{2\nu}) \mu_{13}^2 + (1 - c_{13}^2 P_{e1}^{2\nu}) \mu_{\tau}^2. \quad (12)$$

Here  $\mu_{ii}$  ( $i = 1, 2, 3$ ) and  $\mu_{ij}$  ( $i, j = 1, 2, 3$ ) are the relevant elements of the Dirac- and Majorana-type magnetic moment matrices, respectively <sup>1</sup>.

Similarly, as developed in ref. [26] and applied in the refs. [44, 45], the effective magnetic moment for the LMA-MSW solution in terms of the flavor-basis can be expressed as

$$(\mu_{eff}^F)^2 = \langle P^m \rangle_{ee} \mu_e^2 + (1 - \langle P^m \rangle_{ee}) (\cos^2 \theta_{23} \mu_\mu^2 + \sin^2 \theta_{23} \mu_\tau^2) \quad (13)$$

where  $\langle P^m \rangle_{ee}$  is given in Eq. (7) and  $\mu_e, \mu_\mu, \mu_\tau$  are the magnetic moments in the flavor bases.

## V. ANALYSIS AND RESULTS

We follow the BOREXINO's paper of phase-I [6–8] and phase-II [9] and take the number of target electrons per 100 tons,  $N_e = 3.307 \times 10^{31}$  while take the  $pp$  reaction flux from ref. [39] that is also summarized in the Appendix of our recent work [21]. Since the  ${}^7\text{Be}$  and  $pep$  fluxes have a discrete spectra, therefore we treat them as delta functions in our analysis to evaluate the rate in Eq. (14). Following Borexino analysis, we use the high-metallicity SSM flux values  $\phi_{{}^7\text{Be}} = 4.48 \times 10^9 \text{ cm}^{-2} \text{ s}^{-1}$  at 0.862 MeV and  $\phi_{pep} = 1.44 \times 10^8 \text{ cm}^{-2} \text{ s}^{-1}$  at 1.44 MeV in our calculations. For predicted rates for each spectra, we use Eq. (7) and (8) to find the modifications due to the small matter effects to the energy- independent vacuum value of  $\langle P^{vac} \rangle_{ee} = 0.558$  and obtain the values  $\langle P^{pp} \rangle_{ee} = 0.554$  for  $pp$ ,  $\langle P^{{}^7\text{Be}} \rangle_{ee} = 0.536$  for  ${}^7\text{Be}$  and  $\langle P^{pep} \rangle_{ee} = 0.529$  for  $pep$ . We can write down the basic structure of the expected rates to compare them with Borexino's results as

$$R_\nu^i = N_e \int_0^{E_{max}} dE_\nu \phi^i(E_\nu) \left( \sigma_e(E_\nu) \langle P^{mi} \rangle_{ee} + \sigma_{\mu,\tau}(E_\nu) [1 - \langle P^{mi} \rangle_{ee}] \right), \quad (14)$$

where  $\langle P^{mi} \rangle_{ee}$  are given in eq. (7) and (8), with the index  $i$  indicating whether  $vac$ ,  $pp$ ,  ${}^7\text{Be}$  or  $pep$ . The cross-sections  $\sigma_e(E_\nu)$  and  $\sigma_{\mu,\tau}(E_\nu)$  are defined in Eqs. (1), (2) and (3). To find the best-fits values and limits on the parameters  $\vec{\lambda} \equiv (\sin^2 \theta_W, \mu_\nu^{eff}, \langle r_\nu^2 \rangle)$ , we use a  $\chi^2$ - estimator

$$\chi^2(\vec{\lambda}) = \sum_i \frac{(R_{exp}^i - R_{pre}^i (1 + \alpha^i))^2}{(\sigma_{stat}^i)^2} + \left( \frac{\alpha^i}{\sigma_\alpha^i} \right)^2, \quad (15)$$

where  $i$  runs over the solar neutrino sources  $pp$ ,  ${}^7\text{Be}$  and  $pep$ . In eq. (15),  $R_{exp}$  are the experimental event rates observed at Borexino in phase I and phase II with  $\sigma_{stat}$  as the statistical uncertainty for each of the five experiments while  $R_{pre}$  is the predicted event rate corresponding to each experiment calculated from eq. (14). With

<sup>1</sup> Ref. [9] mistakenly put a factor of  $P_{e1}^{2\nu}$  in the first term of eq. (9).

$\mu_\nu^{eff} = 0, \langle r_\nu^2 \rangle = 0$  and the PDG(2016) value  $\sin^2 \theta_W = 0.2313$  [37], our predicted event rate values are  $R^{pp} = 131 \pm 2.4$  ( $144 \pm 13, 134 \pm 10$ ),  $R^{7Be} = 47.8 \pm 2.9$  ( $46 \pm 1.5, 48.3 \pm 1.1$ ) and  $R^{pep} = 2.74 \pm 0.05$  ( $3.1 \pm 0.6, 2.43 \pm 0.36$ ), where the Borexino's phase-I and phase-II measured values are given inside the parentheses, respectively. The measured values for phase-I were taken from ref. [6–8] and for phase-II were taken from ref. [9]. Notice that we have taken the uncertainties of the expected event rates 2.4, 2.9 and 0.05 for pp,  ${}^7\text{Be}$  and pep, respectively, from the TABLE I of ref. [9]. In Eq. (15), we add penalty term corresponding to each experiment to account for the theoretical uncertainties coming from the solar flux models and from the oscillation parameters.

We fit  $\sin^2 \theta_W, \mu_\nu^{eff}$  and  $\langle r_\nu^2 \rangle$  in one and two parameter spaces while minimizing over the pull parameters " $\alpha$ " within  $\sigma_\alpha^i$  where  $\sigma_\alpha^i$  are the relative uncertainties calculated from the total uncertainties (2.4, 2.9 and 0.05) of the predicted event rates given in TABLE I of ref. [9], and also reported above in addition to our predicted event rates. The calculated relative uncertainties used in this analysis are 2%, 6%, 2% for pp,  ${}^7\text{Be}$  and pep fluxes, respectively. We have also included the radiative correction (2%) to the SM cross-section given in Eq. (2). Values of the mixing parameters were taken from PDG(2016) [37]

Using Borexino's published values for the rates in phase-I [6–8] and phase-II [9] and their  $1\sigma$  statistical uncertainties for pp,  ${}^7\text{Be}$  and pep real time detections, we find a best-fit value  $\sin^2 \theta_W = 0.235 \pm 0.019$ , which is consistent with both the low-energy theoretical prediction [46] and with  $\overline{MS}$  value at the Z-boson mass. This result has a slightly weaker precision than those obtained from decay and reactor data studies [12, 22, 47, 48]. Because it includes the pp and  ${}^7\text{Be}$  data, our determination of  $\sin^2 \theta_W = 0.235 \pm 0.01$  is below the energies of its other measurements to date, excepting the recent estimate in ref. [21] for phase-II of Borexino's data. Previously, the lowest energy determinations were the atomic parity violation measurement in  ${}^{133}\text{Cs}$  at 2.4 MeV [10–12].

In Fig. 1, we show the 2-*d.o.f* parameter space of  $\sin^2 \theta_W$  and the neutrino effective magnetic moment  $\mu_\nu^{eff}$  with the 90%, 95% and 99% C.L. boundaries from inner to outer, respectively. In Fig. 2, we demonstrate the 1-dim  $\Delta\chi^2$  distribution of the three unknown parameters,  $\sin^2 \theta_W$  (top),  $\mu_\nu^{eff}$  (middle),  $\langle r_\nu^2 \rangle$  (bottom) with  $1\sigma$  and the 90% C.L. projection on each distribution. The best-fits and bounds of the three parameters at 90% C.L. are  $\sin^2 \theta_W = 0.235 \pm 0.019$ ,  $\mu_\nu^{eff} \leq 8.7 \times 10^{-12} \mu_B$  and  $-0.82 \times 10^{-32} \text{cm}^2 \leq \langle r_\nu^2 \rangle \leq 1.27 \times 10^{-32} \text{cm}^2$  and  $-9 \times 10^{-32} \text{cm}^2 \leq \langle r_{\nu\mu, \nu\tau}^2 \rangle \leq 3.1 \times 10^{-31} \text{cm}^2$ . The two parameter fits in Fig. 1 and one parameter fits in Fig. 2 for  $\sin^2 \theta_W, \mu_\beta^{eff}$  and for  $\langle r_{\nu e}^2 \rangle$  and  $\langle r_{\nu\mu}^2 \rangle$  or  $\langle r_{\nu\tau}^2 \rangle$  are consistent with each other. The best-fit parameter values and bounds are also quoted in TABLE I. Notice that we have also carried out an analysis for the phase-II data only and found that upper limit value of  $\mu_\nu^{eff}$  obtained is  $1.3 \times 10^{-11} \mu_B$  which is around a factor of 2 different than the value quoted in ref. [45] by Borexino collaboration. The apparent difference occurs due to the fact that the Borexino collaboration includes both statistical and systematic uncertainties in their analysis while we use only the statistical uncertainties. This could be a good basis of motivation for the Borexino experiment to perform a detailed spectral analysis using the combined data of phase-I and phase-II.

The upper bound value of  $\mu_\nu^{eff}$  at 90% C.L. is then used in Eq. (11) and (12) to derive the values of the Dirac-type and Majorana-type magnetic moment matrix elements by taking one element at-a-time, the relevant parameter values obtained are quoted in TABLE II. Since we have three different solar fluxes with different energies so we derive the matrix element values for each flux separately and marginal differences from lower to higher energy fluxes can be seen from the Table. A similar procedure has been repeated for the neutrino magnetic moment in the flavor basis using Eq. (13) and the values obtained are given in the last three columns of TABLE II.

## VI. CONCLUSIONS

In this paper we have performed event rate analysis to estimate the value of electroweak parameter  $\sin^2 \theta_W$  and electromagnetic parameters of neutrino due to its nonzero size using the lowest available solar neutrino energy spectra of pp,  ${}^7\text{Be}$  and pep from Borexino phase I and phase II runs. We have included both the theoretical model and the measured statistical uncertainties to estimate the best-fit values and bounds of the parameters. The best-fit value of  $\sin^2 \theta_W$  obtained at 90% C.L. was  $0.235 \pm 0.019$  with the precision better than 8%. The precision obtained here is comparable to that obtained from the combined reactor and accelerator very short-baseline experiments [22]. The upper bound obtained for the effective magnetic moment parameter is  $\mu_\nu^{eff} \leq 8.7 \times 10^{-12} \mu_B$  at 90% C.L., which has a factor of 3 improvement compared to the previous bounds. It turns out in improving the bounds of the magnetic moment elements for both the Dirac-type and Majorana-type in the mass and also in the flavor basis by a factor of 3 to 5 as given in TABLE II. Similarly, the bounds on the neutrino charge radii turn out to

be  $-0.82 \times 10^{-32} \text{cm}^2 \leq \langle r_{\nu_e}^2 \rangle \leq 1.27 \times 10^{-32} \text{cm}^2$  and  $-9 \times 10^{-32} \text{cm}^2 \leq \langle r_{\nu_\mu, \nu_\tau}^2 \rangle \leq 3.1 \times 10^{-31} \text{cm}^2$  at 90% C.L..

Current and future solar neutrino low-energy fluxes,  $pp$  and  ${}^7\text{Be}$  in particular, have a strong potential to provide a precise measurement of  $\sin^2 \theta_W$  and higher sensitivity to all of the electromagnetic properties of neutrinos and the related parameters to give decisive information about the nature of neutrinos whether Dirac or Majorana. They can test  $\sin^2 \theta_W = 0.23867 \pm 0.00016$  prediction of  $\overline{MS}$  running of the parameter to the sub-MeV region. Moreover, from the low-energy solar fluxes the electromagnetic parameters of at least two flavors of neutrinos can be constrained and explored as we showed in this work. We anticipate that the Borexino collaboration will carry out a detailed spectral analysis for the combined data of phase I and phase II to confirm the calculations of this work.

### Acknowledgments

The author thanks Prof. Douglas McKay from Kansas University and Prof. Jiajae Ling from Sun Yat-Sen University for their useful suggestions and comments. The financial support for this work has been provided by the Sun Yat-Sen University under the Postdoctoral Fellowship program, the China Postdoctoral Science Foundation under the grant # 74130-41090002 and the NPC fellowship award, Neutrino Physics Center, Fermilab.

- 
- [1] The CMS Collaboration, PAS SMP-16-007, (2017).
  - [2] G. Aad *et al.*, (The ATLAS collaboration), JHEP 09 (2015) 049
  - [3] R. Aaij *et al.*, (The LHCb collaboration), JHEP 1511(2015) 190
  - [4] B. Aharmim *et al.*, [SNO Collab.], Phys. Rev. Lett. 101, 111301 (2008); Phys. Rev. C87, 015502 (2013).
  - [5] K. Eguchi *et al.*, [KamLAND Collab.], Phys. Rev. Lett. 90, 021802 (2003), Phys. Rev. Lett. 94, 081801 (2005).
  - [6] G. Bellini *et al.* (Borexino Collaboration), Nature **512**, 383 (2014)
  - [7] G. Bellini *et al.* (Borexino Collaboration), Phys. Rev. Lett. **107**, 141302 (2011).
  - [8] G. Bellini *et al.* (Borexino Collaboration), Phys. Rev. Lett. **108**, 051302 (2012).
  - [9] M. Agostini *et al.* (Borexino Collaboration), arXiv:1707.09279v1.
  - [10] C. Bouchiat and S.A. Piketty, Phys. Lett. B, 128, 73 (1983).
  - [11] C. S. Wood *et al.*, Science **275**, 1759 (1997).
  - [12] S. G. Porsev, K. Bely and A. Derevianko, Phys. Rev. Lett. **102**, 181601 (2009).
  - [13] R. Aaij *et al.*, (The LHCb collaboration), JHEP 08 (2017) 055
  - [14] R. Aaij *et al.*, (The LHCb collaboration), PRL 113 (2014) 151601
  - [15] Lorenzo Calibbi and Giovanni Signorelli, arXiv:1709.00294v1
  - [16] <http://www.slac.stanford.edu/xorg/hflav/semi/fpcp17/RDRDs.html> and references therein.
  - [17] D. Androic, (Qweak Collaboration), PRL 111, 141803 (2013)
  - [18] T. Allison, (Qweak Collaboration), arXiv:1409.7100v2.
  - [19] The SoLID Collaboration, SoLID (Solenoidal Large Intensity Device) Preliminary Conceptual Design Report, May, 2014 ([http://hallweb.jlab.org/12GeV/SoLID/download/doc/solid\\_precedr.pdf](http://hallweb.jlab.org/12GeV/SoLID/download/doc/solid_precedr.pdf)).
  - [20] J. Benesch, (The MOLLER Collaboration), arXiv:1411.4088v2
  - [21] Amir N. Khan and Douglas W. McKay, JHEP 1707 (2017) 143, arXiv:1704.06222v2
  - [22] A. N. Khan, Phys. Rev. D **93**, 093019(2016).
  - [23] F. An *et al.* (JUNO Collaboration), J. Phys. G **43**, 03040 (2016); arXiv:1507.05613
  - [24] K. Abe *et al.* (Hyper-Kamiokande Collaboration), arXiv:1109.3262v1
  - [25] J. Beacom *et al.* (The CJPL Collaboration), arXiv:1602.01733v4.
  - [26] P. Vogel and J. Engel, Phys. Rev. **D39**, 3378 (1989).
  - [27] C. Giunti and A. Studenikin, Rev. Mod. Phys. **87** 531, (2015).
  - [28] W. A. Bardeen, R. Gastmans and B. Lautrup, Nucl.Phys. **B46**, 319 (1972).
  - [29] M. Dvornikov and A. Studenikin, Phys. Rev. **D69**, 073001 (2004), hep-ph/0305206.
  - [30] M. Dvornikov and A. Studenikin, J. Exp. Theor. Phys. **99**, 254 (2004), hep-ph/0411085.
  - [31] S. Lee, Phys.Rev. **D6**, 1701 (1972).
  - [32] B. W. Lee and R. E. Shrock, Phys. Rev. **D16**, 1444 (1977).
  - [33] J. Bernabeu, L. G. Cabral-Rosetti, J. Papavassiliou and J. Vidal, Phys. Rev. **D62**, 113012 (2000), hep-ph/0008114.
  - [34] J. Bernabeu, J. Papavassiliou and J. Vidal, Phys. Rev. Lett. **89**, 101802 (2002), hep-ph/0206015.
  - [35] J. Bernabeu, J. Papavassiliou and J. Vidal, Nucl. Phys. **B680**, 450 (2004), hep-ph/0210055.
  - [36] J. Barranco *et al.* / Physics Letters **B 662** (2008) 431–435.
  - [37] K. Nakamura and S.T. Petcov, in Patrignani *et al.*, PDG, Chin. Phys. **C 40**, 100001 (2016) and 2017 update.
  - [38] I. Lopes and S. Turck-Chieze, Astrophys. J. **765**, 14 (2013).
  - [39] J. N. Bahcall, M. Kamionkowski and A. Sirlin, Phys. Rev. **D 51**, 6146 (1995).
  - [40] B. Kayser, Phys. Rev. **D26**, 1662 (1982).



- [41] R.E. Shrock, Nucl. Phys. B206, 359 (1982).
- [42] B. C. Cañas, O. G. Miranda, A. Parada, M. Tórtolac, J.W.F. Valle, Physics Letters B 753(2016)191–198
- [43] W. Grimus et al. Nucl. Phys. B 646, 376 (2003)
- [44] D. Montanino, M. Picariello and J. Pulido, Phys. Rev. D77, 093011, (2008).
- [45] M. Agostini *et al.* (Borexino Collaboration), arXiv:1707.09355v2
- [46] J. Erler and M. J. Ramsey-Musolf, Phys. Rev. D 72, 073003 (2005).
- [47] M. Deniz *et al.* (TEXONO Collaboration), Phys. Rev. D 82, 033004 (2010).
- [48] B. C. Canas, E. A. Garces, O. G. Miranda, M. Tortola and J. W. F. Valle, Phys. Lett. B 761, 450 (2016).
- [49] J. F. Beacom and P. Vogel, Phys. Rev. Lett. 83, 5222-5225, (1999).